Acta of Bioengineering and Biomechanics
Vol. 11, No. 2, 2009

Original paper

Hydrodynamic pressure, carrying capacities, friction forces in biobearing gap

KRZYSZTOF CH. WIERZCHOLSKI

Institute of Mechatronics, Nanotechnology and Vacuum Technique, Technical University of Koszalin, Koszalin, Poland.

The present paper deals with the calculations of the pressure distributions, carrying capacities and friction forces derivations in a super-thin layer of biological synovial fluid inside the slide biobearing gap limited by a spherical, conical, cylindrical, parabolic, hyperbolic bone heads. There are also described unsteady and random flow conditions of the bio-bearing lubrication with the changes of the dynamic viscosity of the synovial fluid in the gap height in general.

Key words: *tribology of biobearing, curvilinear biobearing shapes, capacities, friction forces*

1. Introduction

The lubrication of biobearing surfaces is limited by various cylindrical, spherical, conical, parabolic, hyperbolic geometries (see figures 1, 2, 3). Friction between biosurfaces is reduced by interposing a layer of non-Newtonian fluids. Figure 3 shows the geometries of cylindrical, spherical, conical, hyperbolic and parabolic bearing surfaces.

The aims of the paper were to find numerical pressure distributions in a thin layer of non-Newtonian syno-

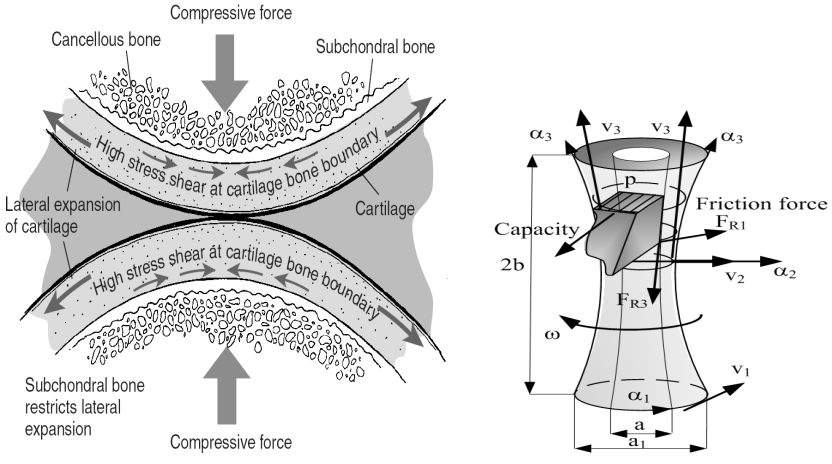

Fig. 1. Human joints: a) fragment of two cooperating cylindrical surfaces of human knee joint, b) fragment of cooperating hyperbolic surfaces of human elbow joint

* Corresponding author: Krzysztof Ch. Wierzcholski, Institute of Mechatronics, Nanotechnology and Vacuum Technique, Technical University of Koszalin, ul. Racławicka 15–17, 75-620 Koszalin, Poland.

Received: April 21st, 2009
Accepted for publication: June 28th, 2009

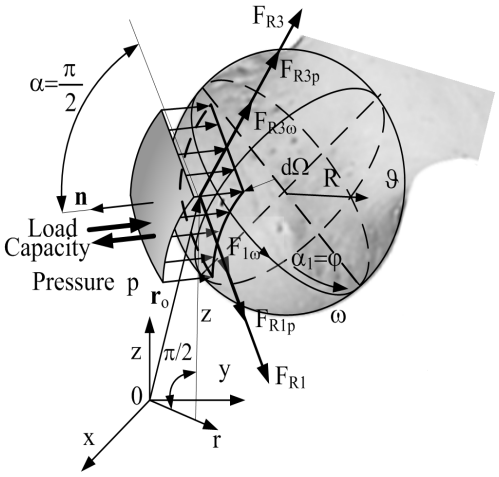

Fig. 2. Human spherical hip joint and schematic location of friction and capacity forces

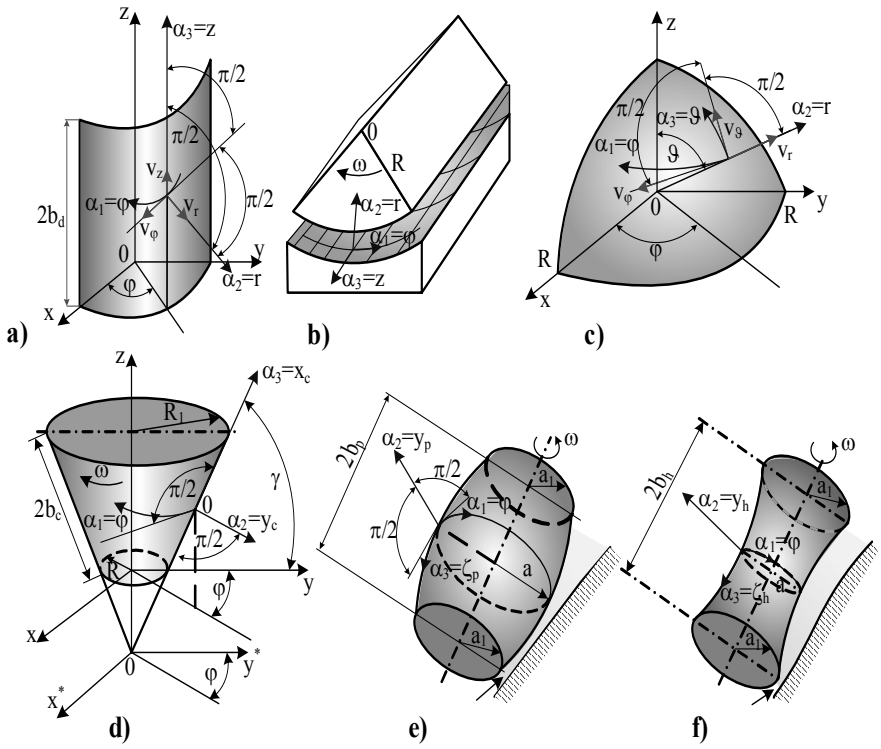

Fig. 3. A view of curvilinear orthogonal biobearing: a), b) cylindrical surfaces, c) spherical surface, d) conical surface, e) parabolic surface, f) hyperbolic surface

vial fluid and to derive friction forces for various biobearing shapes. Dynamic viscosity of the fluid changes in the plane of bearing surface and in gap height direction. This paper generalizes the achievements in the field of biobearing, obtained recently [1]–[6], [15]–[18]. Random conditions are taken into account.

A general idea of the investigations presented in this paper is to establish the influence of bone head shapes in human joints on their carrying capacity values. Moreover, there is presented the influence of impulsive time-dependent synovial fluid flow in joint gap on the carrying capacity distributions in stochastic changes of cartilage roughness with optimum standard deviation.

2. Basic equations

Estimation of dimensionless terms with respect to the boundary simplifications in the equations of conservation of momentum and continuity equation in the

curvilinear orthogonal co-ordinates α_1, α_2, α_3, for incompressible, non-stationary and unsymmetrical lubricant flow in thin layer resting on rotational surface of biobearing gap, with non-monotonic generating line, leads to the following system of basic equations [10], [11], [14], [18]:

$$\rho\frac{dv_1}{dt}=-\frac{1}{h_1}\frac{\partial p}{\partial\alpha_1}+\frac{\partial}{\partial\alpha_2}\left(\eta\frac{\partial v_1}{\partial\alpha_2}\right), \tag{1}$$

$$0=\frac{\partial p}{\partial\alpha_2}, \tag{2}$$

$$\rho\frac{dv_3}{dt}=-\frac{1}{h_3}\frac{\partial p}{\partial\alpha_3}+\frac{\partial}{\partial\alpha_2}\left(\eta\frac{\partial v_3}{\partial\alpha_2}\right), \tag{3}$$

$$0=h_3\frac{\partial v_1}{\partial\alpha_1}+h_1h_3\frac{\partial v_2}{\partial\alpha_2}+\frac{\partial}{\partial\alpha_3}\left(h_1v_3\right), \tag{4}$$

where in the length, width and gap-height directions, we have respectively: $0<\alpha_1\le 2\pi$, $-b_m\le\alpha_3\le b_s$, $0\le\alpha_2\le\varepsilon$. The system of equations (1)–(4) contains the following unknowns: v_1, v_2, v_3, i.e. three dimensional components of synovial fluid velocity vector in three curvilinear, orthogonal dimensional directions: α_1, α_2, α_3, $p(\alpha_1,\alpha_3,t)$ – hydrodynamic dimensional pressure. The symbol α_1 stands for a circumferential direction in each coordinate system, for example, φ in cylindrical or spherical bearings. The symbol α_2 is the gap height direction, for example, r in cylindrical or spherical biobearing. The symbol α_3 indicates a longitudinal direction in each coordinate system, for example, z in cylindrical biobearing and ϑ in spherical ones. Hence we have the fluid velocity components: $(v_1, v_2, v_3) = (v_\varphi, v_r, v_z)$ in cylindrical coordinates, and $(v_1, v_2, v_3) = (v_\varphi, v_r, v_\vartheta)$ in spherical coordinates. We denote: R – the radius of the curvature in α_1 direction, $U=\omega R$ – the surface linear dimensional velocity in α_1 direction, and ε_T – an average dimensional gap height, ω – an angular journal velocity. In a non-classical theory of hydrodynamic lubrication, the dynamic viscosity η of the lubricant depends on circumferential (α_1), longitudinal (α_3) and gap (α_2) height directions [7]–[9]. If the orthogonal curvilinear coordinates α_1, α_2, α_3 are the lines of curvature of a thin layer of lubricant resting on the rotational biobearing surface in gap, where α_1 is a circumferential direction, α_3 – a generating line of rotational surface, α_2 – gap-height direction, then the Lamé coefficients for the thin layer with non-monotonic generating line are as follows [14]:

$$h_1\equiv h_1(\alpha_3),\quad h_2\equiv 1,\quad h_3\equiv h_3(\alpha_3). \tag{5}$$

The synovial fluid flow in biobearing gap is generated by the rotation of the cylindrical, spherical, conical, and parabolic bone heads. The gap height ε_T changes in the gap height direction α_2 with time. Hence the boundary conditions for lubricant velocity components take the form [12], [13]:

$$\begin{aligned} v_1(\alpha_1,\alpha_2,\alpha_3,t)&=\omega h_1 \text{ for } \alpha_2=0,\\ v_1(\alpha_1,\alpha_2,\alpha_3,t)&=0 \text{ for } \alpha_2=\varepsilon_T, \end{aligned} \tag{6}$$

$$\begin{aligned} v_2(\alpha_1,\alpha_2,\alpha_3,t)&=0 \text{ for } \alpha_2=0,\\ v_2(\alpha_1,\alpha_2,\alpha_3,t)&=\partial\varepsilon_T/\partial t \text{ for } \alpha_2=\varepsilon_T, \end{aligned} \tag{7}$$

$$\begin{aligned} v_3(\alpha_1,\alpha_2,\alpha_3,t)&=0 \text{ for } \alpha_2=0,\\ v_3(\alpha_1,\alpha_2,\alpha_3,t)&=0 \text{ for } \alpha_2=\varepsilon_T. \end{aligned} \tag{8}$$

3. Integration method

3.1. Fluid velocity distributions in curvilinear gaps of biobearings

Various shapes of biobearing journals and gaps simulate the capability to control and to attain the desired, best operating parameters. Now we consider the system of equations (1)–(4) in curvilinear orthogonal coordinates for unsteady flow and variable viscosity $\eta(\alpha_1, \alpha_2, \alpha_3)$ [4]. Solutions of the partial differential equations (1)–(4) under the boundary conditions (6), (8) have the following forms [12], [14]:

$$v_1(\alpha_1,\alpha_2,\alpha_3,t)=\frac{1}{h_1}\frac{\partial p}{\partial\alpha_1}A_\eta+(1-A_s)\omega h_1, \tag{9}$$

$$v_3(\alpha_1,\alpha_2,\alpha_3,t)=\frac{1}{h_3}\frac{\partial p}{\partial\alpha_3}A_\eta, \tag{10}$$

whereas

$$\begin{aligned} A_s(\alpha_1,\alpha_2,\alpha_3)&\equiv\frac{\int_0^{\alpha_2}\frac{1}{\eta}d\alpha_2}{\int_0^{\varepsilon_T}\frac{1}{\eta}d\alpha_2},\\ A_\eta(\alpha_1,\alpha_2,\alpha_3)&\equiv\int_0^{\alpha_2}\frac{\alpha_2}{\eta}d\alpha_2-A_s(\alpha_1,\alpha_2,\alpha_3)\int_0^{\varepsilon_T}\frac{\alpha_2}{\eta}d\alpha_2, \end{aligned} \tag{11}$$

where: $0 \le \alpha_1 \le 2\pi\theta_1$, $0 \le \theta_1 \le 1$, $b_{m.} \le \alpha_3 \le b_s$, $0 \le \alpha_2 \le \varepsilon_T$, $\varepsilon_T = \varepsilon_T(\alpha_1, \alpha_3)$, $\eta(\alpha_1, \alpha_2, \alpha_3)$. Solution of the continuity equations under the boundary conditions $(7)_1$, where $v_2 = 0$ for $\alpha_2 = 0$, has the following form [12]:

$$v_2(\alpha_1, \alpha_2, \alpha_3) = -\int_0^{\alpha_2} \frac{1}{h_1}\frac{\partial v_1}{\partial \alpha_1} d\alpha_2 - \int_0^{\alpha_2} \frac{1}{h_1 h_3}\frac{\partial (h_1 v_3)}{\partial \alpha_3} d\alpha_2, \quad (12)$$

where: $0 \le \alpha_1 \le 2\pi\theta_1$, $0 \le \theta_1 \le 1$, $b_m \le \alpha_3 \le b_s$, $0 \le \alpha_2 \le \varepsilon_T$.

3.2. Pressure distributions in curvilinear biobearing gaps

We insert solutions (9), (10) into solution (12) and calculate the expected value of both sides of the equation by using the expectation operator E. If we impose boundary condition $(7)_2$ for radial component of fluid velocity, i.e. $v_2 = \partial\varepsilon_T/\partial t$ for $\alpha_2 = \varepsilon_T$, then it is easy to find out that the pressure function p in the curvilinear coordinates $(\alpha_1, \alpha_2, \alpha_3)$ satisfies the following modified stochastic Reynolds equation [14]:

$$\frac{1}{h_1}\frac{\partial}{\partial \alpha_1}\left[\frac{\partial \mathrm{E}(p)}{\partial \alpha_1}\mathrm{E}\left(\int_0^{\varepsilon_T} A_\eta d\alpha_2\right)\right] + \frac{1}{h_3}\frac{\partial}{\partial \alpha_3}\left[\frac{h_1}{h_3}\frac{\partial \mathrm{E}(p)}{\partial \alpha_3}\mathrm{E}\left(\int_0^{\varepsilon_T} A_\eta d\alpha_2\right)\right] = \omega h_1 \frac{\partial}{\partial \alpha_1}\left[\mathrm{E}\left(\int_0^{\varepsilon_T} A_s d\alpha_2\right) - \mathrm{E}(\varepsilon_T)\right] - h_1 \frac{\partial \mathrm{E}(\varepsilon_T)}{\partial t}, \quad (13)$$

where the dynamic viscosity of oil is not constant in the gap height direction, i.e. $\eta(\alpha_1, \alpha_2, \alpha_3)$. If the dynamic viscosity of synovial fluid is constant in the gap height direction, i.e. $\eta(\alpha_1, \alpha_3)$, then:

$$A_s = \frac{\alpha_2}{\varepsilon_T} \equiv s, \quad \int_0^{\varepsilon_T} A_\eta d\alpha_2 = -\frac{\varepsilon_T^3}{12\eta}, \quad \int_0^{\varepsilon_T} A_s d\alpha_2 - \varepsilon_T = -\frac{1}{2}\varepsilon_T. \quad (14)$$

Hence the stochastic Reynolds equation (13) tends to the following form [14]:

$$\frac{1}{h_1}\frac{\partial}{\partial \alpha_1}\left[\frac{\mathrm{E}(\varepsilon_T^3)}{\eta}\frac{\partial \mathrm{E}(p)}{\partial \alpha_1}\right] + \frac{1}{h_3}\frac{\partial}{\partial \alpha_3}\left[\frac{h_1}{h_3}\frac{\mathrm{E}(\varepsilon_T^3)}{\eta}\frac{\partial \mathrm{E}(p)}{\partial \alpha_3}\right] = 6\omega h_1 \frac{\partial \mathrm{E}(\varepsilon_T)}{\partial \alpha_1} + 12 h_1 \frac{\partial \mathrm{E}(\varepsilon_T)}{\partial t}. \quad (15)$$

The dimensional gap height ε_T depends on the variables α_1 and α_3 and consists of two parts [14]:

$$\varepsilon_T = \varepsilon_{Ts}(\alpha_1, \alpha_3) + \delta(\alpha_1, \alpha_3, \xi), \quad (16)$$

where ε_{Ts} denotes the total dimensional nominal smooth part of geometrical form of a thin fluid layer. This part of the gap height contains dimensional corrections of the gap height caused by the hyper-elastic deformations. The symbol δ stands for the dimensional random part of gap-height changes resulting from vibrations, unsteady loading and surface roughness measured from the nominal mean level. The symbol ξ describes the random variable, which characterizes the roughness arrangement. By using the optimal function f of the probability density distribution of the stochastic gap changes caused by the roughness, the mean value of total film thickness $\mathrm{E}(\varepsilon_T)$ and the mean value of function (*), hence E(*), are represented by virtue of the expectation operator in the following form [14]:

$$\mathrm{E}(*) = \int_{-\infty}^{+\infty} (*) \times f(\delta_1) d\delta_1, \quad \sigma_s = \frac{c_1}{\sqrt{13}} = 0.375, \quad f(\delta_1) \equiv \begin{cases} \left(1 - \dfrac{\delta_1^2}{c_1^2}\right)^5 & \text{for } -c_1 \le \delta_1 \le +c_1, \\ 0 & \text{for } |\delta_1| > c_1, \end{cases} \quad (17)$$

where the symbol $c_1 = 1.353515$ denotes the half total range of random variable of a thin layer thickness of a normal hip joint. The symbol δ_1 stands for the dimensionless random part of the gap height. We have $\delta = \varepsilon_0\delta_1$ and $c = \varepsilon_0 c_1$, where the symbol ε_0 represents a characteristic value of gap height. The dimensionless value of the standard deviation $\sigma_s = 0.37539$ was obtained based on the calculations of real roughness of microbearing surfaces. Using the dimensionless probability function (17), after calculations finally we obtain [14]:

$$\mathrm{E}(\varepsilon_T) = \int_{-c_1}^{+c_1} (\varepsilon_{Ts} + \varepsilon_0\delta_1)\, f(\delta_1) d\delta_1 = \varepsilon_{Ts}, \quad \mathrm{E}(\varepsilon_T^3) = \int_{-c_1}^{+c_1} (\varepsilon_{Ts} + \varepsilon_0\delta_1)^3 f(\delta_1) d\delta_1 = \varepsilon_{Ts}^3 + 3\sigma_s^2 \varepsilon_{Ts}. \quad (18)$$

4. Friction forces in biobearing gap

This section presents the calculations of friction forces in micro- and biobearing gaps.

The time-depended components of friction forces in the curvilinear directions α_1, α_3 in micro- and biobearing gaps have the following forms:

$$F_{R1}(t) = \iint\limits_{\Omega} \left(\eta \frac{\partial v_1}{\partial \alpha_2} \right)_{\alpha_2 = \varepsilon_T} h_1 h_3 d\alpha_1 d\alpha_3,$$
$$F_{R3}(t) = \iint\limits_{\Omega} \left(\eta \frac{\partial v_3}{\partial \alpha_2} \right)_{\alpha_2 = \varepsilon_T} h_1 h_3 d\alpha_1 d\alpha_3, \tag{19}$$

where:

$0 \le \alpha_1 \le 2\pi\theta_1$, $0 \le \theta_1 \le 1$, $b_m \le \alpha_3 \le b_s$, $0 \le \alpha_2 \le \varepsilon_T$, $\varepsilon_T = \varepsilon_T(\alpha_1, \alpha_3)$, $\eta(\alpha_1, \alpha_2, \alpha_3)$,

$\Omega(\alpha_1, \alpha_3)$ – the lubrication surface,

$\varepsilon_T(\alpha_1, \alpha_3)$ – the gap height,

$\eta(\alpha_1, \alpha_2, \alpha_3)$ – the fluid dynamic viscosity,

v_1, v_3 – the components of fluid velocity in α_1, α_3 directions, respectively.

In this intersection, the components F_{R1} and F_{R3} of friction velocity in α_1 and α_3 directions, respectively, will be determined. By virtue of the components of fluid velocity (9), (10), the components (19) of friction forces are as follows [18]:

$$F_{R1} = \iint\limits_{\Omega} \left[\frac{\eta(\alpha_1, \alpha_2, \alpha_3)}{h_1} \frac{\partial p}{\partial \alpha_1} \frac{\partial A_\eta(\alpha_1, \alpha_2, \alpha_3)}{\partial \alpha_2} \right]_{\alpha_2 = \varepsilon_T} h_1 h_3 d\alpha_1 d\alpha_3 - \iint\limits_{\Omega} \left[\omega h_1 \eta(\alpha_1, \alpha_2, \alpha_3) \frac{\partial A_s(\alpha_1, \alpha_2, \alpha_3)}{\partial \alpha_2} \right]_{\alpha_2 = \varepsilon_T} h_1 h_3 d\alpha_1 d\alpha_3, \tag{20}$$

$$F_{R3} = \iint\limits_{\Omega} \left[\frac{\eta(\alpha_1, \alpha_2, \alpha_3)}{h_3} \frac{\partial p}{\partial \alpha_3} \frac{\partial A_\eta(\alpha_1, \alpha_2, \alpha_3)}{\partial \alpha_2} \right]_{\alpha_2 = \varepsilon_T} h_1 h_3 d\alpha_1 d\alpha_3 . \tag{21}$$

If the functions A_s, A_η from formulae (11) are inserted into (20), (21), then the components of friction force can be put in the form [18]:

$$F_{R1} = \iint\limits_{\Omega} \frac{1}{h_1} \frac{\partial p}{\partial \alpha_1} \left[\varepsilon_T(\alpha_1, \alpha_3) - \frac{\int_0^{\varepsilon_T(\alpha_1, \alpha_3)} \frac{\alpha_2 d\alpha_2}{\eta(\alpha_1, \alpha_2, \alpha_3)}}{\int_0^{\varepsilon_T(\alpha_1, \alpha_3)} \frac{d\alpha_2}{\eta(\alpha_1, \alpha_2, \alpha_3)}} \right] h_1 h_3 d\alpha_1 d\alpha_3 - \iint\limits_{\Omega} \left[\frac{\omega h_1^2 h_3}{\int_0^{\varepsilon_T(\alpha_1, \alpha_3)} \frac{d\alpha_2}{\eta(\alpha_1, \alpha_2, \alpha_3)}} \right] d\alpha_1 d\alpha_3, \tag{22}$$

$$F_{R3} = \iint\limits_{\Omega} \frac{1}{h_3} \frac{\partial p}{\partial \alpha_3} \left[\varepsilon_T(\alpha_1, \alpha_3) - \frac{\int_0^{\varepsilon_T(\alpha_1, \alpha_3)} \frac{\alpha_2 d\alpha_2}{\eta(\alpha_1, \alpha_2, \alpha_3)}}{\int_0^{\varepsilon_T(\alpha_1, \alpha_3)} \frac{d\alpha_2}{\eta(\alpha_1, \alpha_2, \alpha_3)}} \right] h_1 h_3 d\alpha_1 d\alpha_3, \tag{23}$$

where: $0 \le \alpha_1 \le 2\pi\theta_1$, $0 \le \theta_1 \le 1$, $b_m \le \alpha_3 \le b_s$, $0 \le \alpha_2 \le \varepsilon_T$, $\varepsilon_T = \varepsilon_T(\alpha_1, \alpha_3)$, $\eta(\alpha_1, \alpha_2, \alpha_3)$.

If a dynamic viscosity of the fluid does not change in the gap-height direction, then formulae (22), (23) tend to the following forms [18]:

$$F_{R1} = \iint_{\Omega} \frac{h_3}{2} \varepsilon_T(\alpha_1, \alpha_3) \frac{\partial p}{\partial \alpha_1} d\alpha_1 d\alpha_3 - \iint_{\Omega} \frac{\omega h_1^2 \eta(\alpha_1, \alpha_3) h_3 d\alpha_1 d\alpha_3}{\varepsilon_T(\alpha_1, \alpha_3)}, \quad (24)$$

$$F_{R3} = \iint_{\Omega} \frac{h_1}{2} \varepsilon_T(\alpha_1, \alpha_3) \frac{\partial p}{\partial \alpha_3} d\alpha_1 d\alpha_3, \quad (25)$$

where: $0 \le \alpha_1 \le 2\pi\theta_1$, $0 \le \theta_1 \le 1$, $b_m \le \alpha_3 \le b_s$, $0 \le \alpha_2 \le \varepsilon_T$, $\eta(\alpha_1, \alpha_3)$.

5. Particular solutions for pressure and friction forces

5.1. Biobearings with cylindrical bone head

For cylindrical biobearing we have $\alpha_1 = \varphi$, $\alpha_2 = r$, $\alpha_3 = z$, and the Lamé coefficients are as follows: $h_1 = R$, $h_3 = 1$, where R is the radius of the bone head (see figure 3a, b). In this case, the modified stochastic Reynolds equations (13), (15) and the friction components (22)–(25) determine the dimensional pressure function $p(\varphi, z, t)$ and the components friction force $F_{R\varphi}(\varphi, z, t)$, $F_{Rz}(\varphi, z, t)$, respectively, in cylindrical coordinates (φ, z). The components of both pressure and friction are valid for fluid dynamic viscosity changes $\eta = \eta(\varphi, r, z)$ in the gap height direction and for the case where viscosity $\eta = \eta(\varphi, z)$ is constant in gap height direction, respectively [18]. Cylindrical biobearing surfaces are shown in figure 1a, b.

5.2. Biobearings with spherical bone head

Spherical bone head is represented by spherical coordinates $\alpha_1 = \varphi$, $\alpha_2 = r$, $\alpha_3 = \vartheta$, and the Lamé coefficients: $h_1 = R\sin\vartheta_1$, $h_3 = 1$, where R is the radius of the sphere (see figure 3c). In this case, the modified stochastic Reynolds equations (13), (15) and the friction components (22)–(25) determine the dimensional pressure function $p(\varphi, \vartheta, t)$ and the friction force components $F_{R\varphi}(\varphi, \vartheta, t)$, $F_{R\vartheta}(\varphi, \vartheta, t)$, respectively, in the spherical coordinates (φ, ϑ).

The components of the pressure and friction are valid for fluid dynamic viscosity changes $\eta = \eta(\varphi, r, \vartheta)$ in gap-height direction and for the case where the viscosity $\eta = \eta(\varphi, \vartheta)$ is constant in the gap-height direction, respectively, [18]. Spherical biobearings are illustrated in figures 1c and 2.

5.3. Biobearings with conical bone head

For the conical biobearing we have $\alpha_1 = \varphi$, $\alpha_2 = y_c$, $\alpha_3 = x_c$ and the dimensional Lamé coefficients are as follows: $h_1 = R + x_c\cos\gamma \equiv X_c$, $h_3 = 1$, where: γ – the angle between conical surface and the cross section plane of the bone head, b_c – the length of the cone-generating line, R – the radius of the bone head (see figure 3d). In this case, the modified stochastic Reynolds equations (13), (15) and the friction components (22)–(25) determine the dimensional pressure function $p(\varphi, x_c, t)$ and the components of the friction force $F_{R\varphi}(\varphi, x_c, t)$, $F_{Rx}(\varphi, x_c, t)$, respectively, in the conical coordinates (φ, x_c). The components of the pressure and friction are valid for the fluid dynamic viscosity changes $\eta = \eta(\varphi, y_c, x_c)$ in the gap-height direction and for the case where the viscosity $\eta = \eta(\varphi, x_c)$ is constant in the gap-height direction, respectively [18]. Conical biobearings are given in figures 1d and 3.

5.4. Biobearings with parabolic and hyperbolic bone heads

For the parabolic biobearing we have $\alpha_1 = \varphi$, $\alpha_2 = y_p$, $\alpha_3 = \zeta_p$, and the non-monotonic generating line of the bone head in the length direction is taken into account. The parabolic biobearing is represented by the following dimensional Lamé coefficients [18]:

$$h_1 = a\cos^2(\Lambda_{p1}\zeta_{p1}),$$
$$h_3 = \sqrt{1 + 4(\Lambda_{p1}/L_{R1})^2 \sin^2(\Lambda_{p1}\zeta_{p1})}\,\cos(\Lambda_{p1}\zeta_{p1}), \quad (26)$$
$$\Lambda_{p1} \equiv \sqrt{\frac{a - a_1}{a}}, \quad L_{R1} \equiv \frac{b_p}{a}, \quad \zeta_{p1} = \frac{\zeta_p}{b_p},$$

where: a – the longest radius of the parabolic bone head, a_1 – the shortest radius of the parabolic bone head, $2b_p$ – the biobearing length (see figure 3e). In this case, the modified stochastic Reynolds equations (13), (15) and the friction components (22)–(25) determine the dimensional pressure function $p(\varphi, \zeta_p, t)$ and the components of the friction force $F_{R\varphi}(\varphi, \zeta_p, t)$, $F_{R\zeta p}(\varphi, \zeta_p, t)$, respectively, in the parabolic coordinates (φ, ζ_p). The components of both pressure and friction are valid for the fluid dynamic viscosity changes $\eta =$

$\eta(\varphi, y_p, \zeta_p)$ in the gap-height direction and for the case where the viscosity $\eta = \eta(\varphi, \zeta_p)$ is constant in the gap-height direction, respectively, [18]. Parabolic biobearings are illustrated in figure 3e.

For the hyperbolic bearing we have $\alpha_1 = \varphi$, $\alpha_2 = y_h$, $\alpha_3 = \zeta_h$, and the non-monotonic generating line of the bone head in length direction is taken into account. The hyperbolic biobearing is represented by the following Lamé coefficients [18]:

$$\begin{gathered} h_1 = a\cos^{-2}(\Lambda_{h1}\zeta_{h1}), \\ h_3 = \sqrt{1+4(\Lambda_{h1}/L_{R1})^2\tan^2(\Lambda_{h1}\zeta_{h1})}\,\cos^{-2}(\Lambda_{h1}\zeta_{h1}), \\ \Lambda_{h1} \equiv \sqrt{\frac{a_1-a}{a}}, \quad L_{R1} \equiv \frac{b_h}{a}, \quad \zeta_{h1} = \frac{\zeta_h}{b_h}, \end{gathered} \tag{27}$$

where: a_1 – the longest radius of the hyperbolic bone head, a – the shortest radius of the hyperbolic bone head, $2b_h$ – the bone head length. In this case, the modified stochastic Reynolds equations (13), (15) and the friction components (22)–(25) determine the dimensional pressure function $p(\varphi, \zeta_h, t)$ and the friction force components $F_{R\varphi}(\varphi, \zeta_h, t)$, $F_{R\zeta h}(\varphi, \zeta_h, t)$, respectively, in the hyperbolic coordinates (φ, ζ_h). The components of both pressure and friction are valid for the fluid dynamic viscosity changes $\eta = \eta(\varphi, y_h, \zeta_h)$ in the gap-height direction and for the case where viscosity $\eta = \eta(\varphi, \zeta_h)$ is constant in the gap-height direction, respectively, [18]. Hyperbolic microbearings are shown in figure 3f.

6. Carrying capacities and friction coefficients in biobearing gap

6.1. Carrying capacities and friction coefficients in cylindrical bio- and microbearings

The carrying capacities in cylindrical bearing are calculated from the following formula [14], [19]:

$$C_{\text{tot}}^{\text{cyl}} = \sqrt{\left[\int_{-b_d}^{+b_d}\left(\int_0^{\varphi_k} p(\varphi,z)R(\sin\varphi)d\varphi\right)dz\right]^2 + \left[\int_{-b_d}^{+b_d}\left(\int_0^{\varphi_k} p(\varphi,z)R(\cos\varphi)d\varphi\right)dz\right]^2}, \tag{28}$$

where φ_k denotes the end coordinate of the film in a circumferential direction and $0 \le \varphi \le 2\pi$, $-b_d \le z \le b_d$, $\varepsilon_T = \varepsilon_T(\varphi, z)$, $2b_d$ is the bearing length.

Friction coefficients in cylindrical coordinates are as follows [18]:

$$\mu_{\text{cyl}} = \frac{|\,\mathbf{e}_\varphi F_{R\varphi} + \mathbf{e}_z F_{Rz}\,|}{C_{\text{tot}}^{\text{cyl}}}, \tag{29}$$

where $\mathbf{e}_\varphi$, $\mathbf{e}_z$ are the unit vectors in the cylindrical φ and z coordinate directions.

6.2. Carrying capacities and friction coefficients in spherical bio- and microbearings

The carrying capacities in spherical bearing are calculated from the following formula:

$$C_{\text{tot}}^{\text{sph}} = \sqrt{\left[\int_{R\pi/8}^{R\pi/2}\left(\int_0^{\varphi_k} p(\varphi,\vartheta)R(\sin\varphi)\sin\left(\frac{\vartheta}{R}\right)d\varphi\right)d\vartheta\right]^2 + \left[\int_{R\pi/8}^{R\pi/2}\left(\int_0^{\varphi_k} p(\varphi,\vartheta)R(\cos\varphi)\sin\left(\frac{\vartheta}{R}\right)d\varphi\right)d\vartheta\right]^2}, \tag{30}$$

where φ_k is the end coordinate of the film in circumferential direction and $0 \le \varphi < 2\pi\theta_1$, $0 \le \theta_1 < 1$, $R\pi/8 \le \vartheta \le R\pi/2$, $\vartheta = R\vartheta_1$.

The friction coefficients in spherical coordinates are as follows [18]:

$$\mu_{\text{sph}} = \frac{|\mathbf{e}_{\varphi} F_{R\varphi} + \mathbf{e}_{\vartheta} F_{R\vartheta}|}{\mathrm{C}_{\text{tot}}^{\text{sph}}}, \tag{31}$$

where $\mathbf{e}_{\varphi}$, $\mathbf{e}_{\vartheta}$ are the unit vectors in the spherical φ and ϑ coordinate directions.

6.3. Carrying capacities and friction coefficients in conical bio- and microbearings

The carrying capacities in conical bearing are calculated from the following formula:

$$C_{\text{tot}}^{\text{con}} = \left\{ \left[\int_0^{+2b_c} \left(\int_0^{\varphi_k} p(\varphi, x_c)(R\sin\varphi + x_c \sin\varphi\cos\gamma) d\varphi \right) dx_c \right]^2 \right.$$

$$\left. + \left[\int_0^{2b_c} \left(\int_0^{\varphi_k} p(\varphi, x_c)(R\cos\varphi + x_c \cos\varphi\cos\gamma) d\varphi \right) dx_c \right]^2 \right\}^{0.5}, \tag{32}$$

where the symbol φ_k denotes the end coordinate of the film in circumferential direction and $0 \le \varphi < 2\pi\theta_1$, $0 \le \theta_1 < 1$, $0 \le x_c \le 2b_c$.

The friction coefficients in conical coordinates are as follows [18]:

$$\mu_{\text{con}} = \frac{|\mathbf{e}_{\varphi} F_{R\varphi} + \mathbf{e}_{x} F_{Rx}|}{\mathrm{C}_{\text{tot}}^{\text{con}}}, \tag{33}$$

where $\mathbf{e}_{\varphi}$, $\mathbf{e}_{x}$ are the unit vectors in the conical φ and x coordinate directions.

6.4. Carrying capacities and friction coefficients in parabolic bio- and microbearings

The carrying capacities in parabolic bearing are calculated from the following formula [19]:

$$C_{\text{tot}}^{\text{par}} = a\left\{ \left[\int_{-b_p}^{+b_p} \left(\int_0^{\varphi_k} p(\varphi, \zeta_p) \sin\varphi \, d\varphi \right) \cos^3\left(\frac{\zeta_p}{b_p} \sqrt{\frac{a-a_1}{a}} \right) \sqrt{1 + 4a \frac{(a-a_1)}{b_p^2} \sin^2\left(\frac{\zeta_p}{b_p} \sqrt{\frac{a-a_1}{a}} \right)} d\zeta_p \right]^2 \right.$$

$$\left. + \left[\int_{-b_p}^{+b_p} \left(\int_0^{\varphi_k} p(\varphi, \zeta_p) \cos\varphi \, d\varphi \right) \cos^3\left(\frac{\zeta_p}{b_p} \sqrt{\frac{a-a_1}{a}} \right) \sqrt{1 + 4a \frac{(a-a_1)}{b_p^2} \sin^2\left(\frac{\zeta_p}{b_p} \sqrt{\frac{a-a_1}{a}} \right)} d\zeta_p \right]^2 \right\}^{0.5}, \tag{34}$$

where φ_k denotes the end coordinate of the film in circumferential direction and $0 \le \varphi < 2\pi\theta_1$, $0 \le \theta_1 < 1$, $\zeta_{p1} = \zeta_p / b_p$, $-b_p \le \zeta_p \le b_p$.

The friction coefficients are as follows [18]:

$$\mu_{\text{par}} = \frac{|\mathbf{e}_{\varphi} F_{R\varphi} + \mathbf{e}_{\zeta_p} F_{R\zeta_p}|}{C_{\text{tot}}^{\text{par}}}, \tag{35}$$

where $\mathbf{e}_{\varphi}$, $\mathbf{e}_{\zeta}$ are the unit vectors in the parabolic φ and ζ_p coordinate directions.

6.5. Carrying capacities and friction coefficients in hyperbolic bio- and microbearings

The carrying capacities in hyperbolic bearing are calculated from the following formula:

$$C_{\text{tot}}^{\text{hyper}} = a\left\{\int_{-b_h}^{+b_h}\left[\left(\int_0^{\varphi_k} p(\varphi,\zeta_h)\sin\varphi d\varphi\right)\cos^{-4}\left(\frac{\zeta_h}{b_h}\sqrt{\frac{a_1-a}{a}}\right)\right.\right.$$

$$\left.\cdot\sqrt{1+4a\frac{(a_1-a)}{b_h^2}\tan^2\left(\frac{\zeta_h}{b_h}\sqrt{\frac{a_1-a}{a}}\right)}d\zeta_h\right]^2$$

$$+\left[\int_{-b_h}^{+b_h}\left(\int_0^{\varphi_k} p(\varphi,\zeta_h)\sin\varphi d\varphi\right)\cos^{-4}\left(\frac{\zeta_h}{b_h}\sqrt{\frac{a_1-a}{a}}\right)\right.$$

$$\left.\left.\cdot\sqrt{1+4a\frac{(a_1-a)}{b_h^2}\tan^2\left(\frac{\zeta_h}{b_h}\sqrt{\frac{a_1-a}{a}}\right)}d\zeta_h\right]^2\right\}^{0.5}, \tag{36}$$

where symbol φ_k denotes the end coordinate of the film in circumferential direction and $0 \le \varphi < 2\pi\theta_1$, $0 \le \theta_1 < 1$, $\zeta_{h1} = \zeta_h/b_p$, $-b_h \le \zeta_h \le b_h$.

The friction coefficients are as follows [18]:

$$\mu_{\text{hyper}} = \frac{|\mathbf{e}_\varphi F_{R\varphi} + \mathbf{e}_{\zeta_h} F_{R\zeta_h}|}{C_{\text{tot}}^{\text{hyper}}}, \tag{37}$$

where $\mathbf{e}_\varphi$, $\mathbf{e}_\zeta$ are the unit vectors in parabolic φ and ζ_h coordinate directions.

7. Numerical calculations

7.1. Numerical calculations of pressure distribution and carrying capacities in cylindrical elbow human joints

As can be seen, human elbow joint is cylindrical in shape. The gap height of a cylindrical biobearing can be written as

$$\varepsilon_T = \varepsilon(1 + \lambda_{cy}\cos\varphi), \tag{38}$$

where: λ_{cy} – the eccentricity ratio in cylindrical microbearing, ε – the radial clearance in cylindrical biobearing. In performed calculations we assume the real geometrical and dynamical values of human elbow joint, namely: the radius of cylindrical bone R = 0.026 m, the length/radius ratio L_{d1} = 1.0, the dynamic viscosity of synovial fluid η_0 = 0.15 Pas, the angular velocity ω = 1.0 s^{-1}, an average value of the pressure $p_0 = \omega\eta_0 R^2/\varepsilon^2 \approx 0.15$ MPa, eccentricity ratio λ_{cy} = 0.7; λ_{cy} = 0.8; λ_{cy} = 0.9.

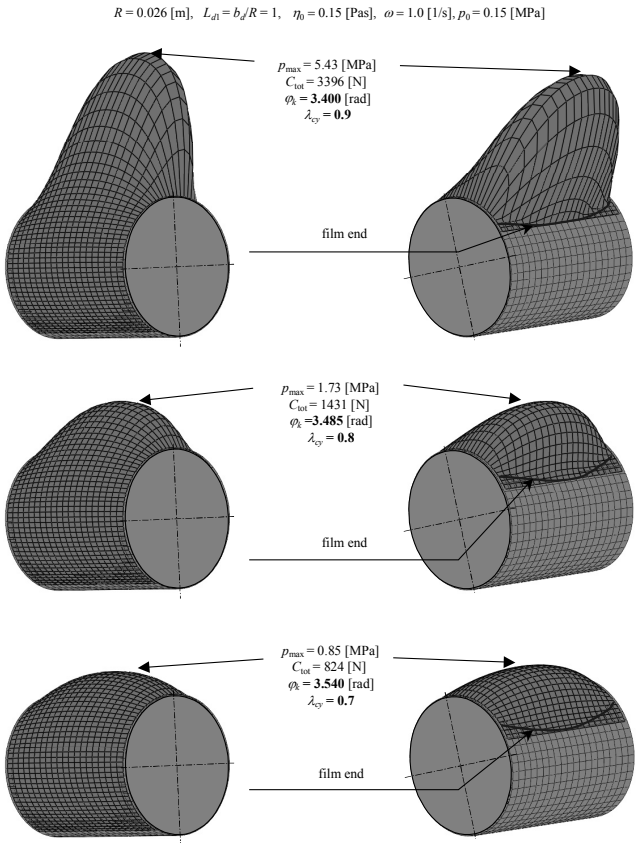

Fig. 4. Dimensional distributions of pressure in cylindrical biobearing (human elbow joint) caused by rotation in circumferential direction where dynamic viscosity of synovial fluid is constant in gap-height direction and stochastic effects are neglected

By virtue of the boundary Reynolds conditions we assume that the angular coordinate of the film end assumes the following values: φ_k = 3.400 rad; φ_k = 3.485 rad; φ_k = 3.540 rad. The pressure distributions and the capacity values in human elbow cylindrical joints are determined in the lubrication region Ω_d, which is defined by the following inequalities: $0 \le \varphi \le \varphi_k$, $-b_d \le z \le b_d$, where $2b_d$ is the length of human elbow joint. Figure 4 presents the pressure distribution in the gap of cylindrical human elbow joint and its total capacity. Numerical calculations of pressure without stochastic changes are shown in figure 4.

Numerical calculations of hydrodynamic pressure and carrying capacities are performed in Matlab 7.2 Professional Program by virtue of equations (15), (28)

for a constant dynamic viscosity in the gap-height direction, by means of the finite difference method. By virtue of the calculations we can see that if the eccentricity ratio increases from 0.7 to 0.9, then the maximum value of hydrodynamic pressure increases from 0.85 MPa to 5.43 MPa and a total carrying capacity value increases from 824 N to 3396 N.

7.2. Numerical calculations of pressure distribution and carrying capacities in human elbow and foot conical joints

The pressure distribution and carrying capacity values in the gap of human elbow, phalange, food conical human joint, are presented, being conical in shape.

The gap height of the conical microbearing and biobearing is defined by

$$\varepsilon_T = \varepsilon(1 + \lambda_c \cos\varphi)\sin^{-1}\gamma, \quad \gamma \neq 0, \tag{39}$$

where λ_c – the eccentricity ratio in conical microbearing, ε – the radial clearance of conical microbearing or biobearing and γ – the angle between generating line and the horizontal y-axis.

Numerical calculations are performed in Matlab 7.2 Professional Program by virtue of the equations (15), (32), for constant dynamic viscosity in gap-height direction, by means of the finite difference method. In these calculations we assume: the least value of the radius of the conical bone R = 0.026 m, the length/radius ratio $L_{c1} = b_c/R = 1$, the dynamic viscosity of the synovial fluid η_0 = 0.15 Pas, the angular velocity ω = 1.0 s^{-1}, the average value of hydrodynamic pressure $p_0 = \omega\eta_0 R^2/\varepsilon^2 \approx 0.15$ MPa, and the following eccentricity ratios λ_c = 0.7; λ_c = 0.8; λ_c = 0.9. By virtue of the boundary Reynolds conditions the angular coordinate of the film end has the values: φ_k = 3.408 rad; φ_k = 3.489 rad; φ_k = 3.549 rad.

Figure 5 shows the numerical values of pressure in conical biobearing gap at the angle γ = 75° between conical surface and the cross section plane without stochastic changes.

From the calculations we can see that if the eccentricity ratio λ_c increases from 0.7 to 0.9, then the maximum value of hydrodynamic pressure increases from 0.78 MPa to 5.21 MPa. The total carrying capacity in the y direction increases from 729 N to 2957 N and total carrying capacity in the z direction increases from 194 N to 729 N.

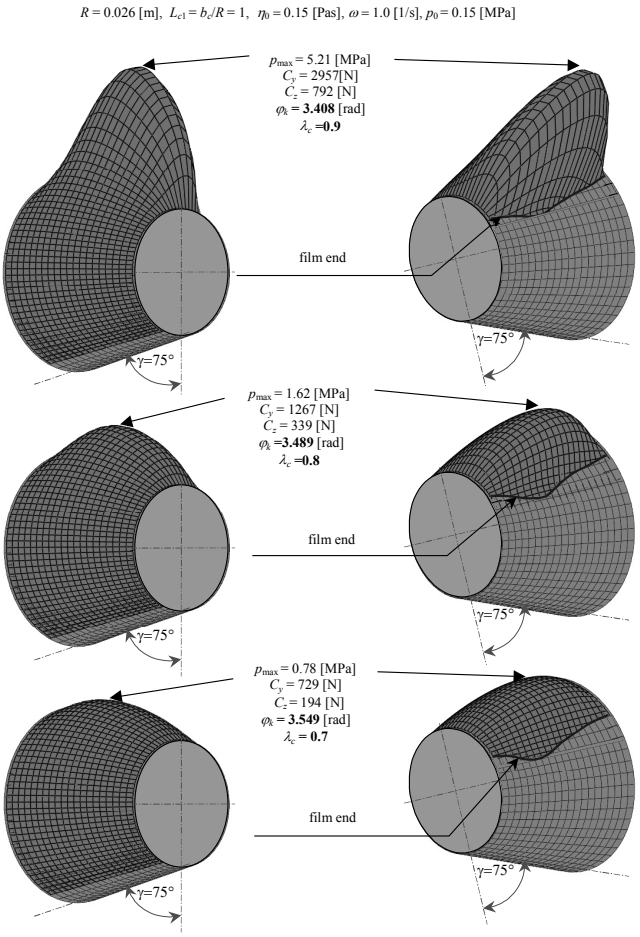

Fig. 5. Dimensional distributions of pressure in conical biobearing caused by rotation in circumferential direction where dynamic viscosity of synovial fluid is constant in gap-height direction and stochastic effects are neglected

7.3. Numerical calculations of pressure distribution and carrying capacities in human hip spherical joints

In the case of impulsive unsteady motion, the dimensionless pressure in the lubrication region Ω $\{0 \leq \varphi < \pi, \pi/8 \leq \vartheta_1 \leq \pi/2]$ is determined. The pressure p_{10} is determined by virtue of the modified stochastic Reynolds equations (13), by taking into account the time-dependent gap height with perturbations and stochastic changes in the following form:

$$\varepsilon_{T1} = \varepsilon_{T1s}(\varphi, \vartheta_1, t_1) + \delta_1$$

$$= \varepsilon_{T1s}(\varphi, \vartheta_1)\,[1 + s_1 \exp(-t_0 t_1 \omega_0)] + \delta_1. \tag{40}$$

The time-independent value of the smooth part of the gap height has the dimensional form:

$$\varepsilon_0\,\varepsilon_{T1s}(\varphi,\,\vartheta_1) = \varepsilon_{Ts}(\varphi,\,\vartheta_1)$$
$$\equiv \Delta\varepsilon_x\cos\varphi\sin\vartheta_1 + \Delta\varepsilon_y\sin\varphi\sin\vartheta_1 - \Delta\varepsilon_z\cos\vartheta_1 - R$$
$$+ [(\Delta\varepsilon_x\cos\varphi\sin\vartheta_1 + \Delta\varepsilon_y\sin\varphi\sin\vartheta_1 - \Delta\varepsilon_z\cos\vartheta_1)^2$$
$$+ (R+\varepsilon_{\min})(R+2D+\varepsilon_{\min})]^{0.5}. \qquad (41)$$

We assume the centre of bone head to be at the point O(0, 0, 0) and the centre of spherical acetabulum at the point $O_1(x - \Delta\varepsilon_x,\ y - \Delta\varepsilon_y,\ z + \Delta\varepsilon_z)$.The eccentricity has the value D (see figure 6).

height, and the characteristic dimensional time t_0 = 0.000001 s. The gap height (41), (42) is taken into account, where such eccentricities of bone head as $\Delta\varepsilon_x$ = 4.0 μm, $\Delta\varepsilon_y$ = 0.5 μm, $\Delta\varepsilon_z$ = 3.0 μm are assumed. In the calculations, we take the optimaum dimensionless standard deviation σ_{s1} = 0.375. We assume that the dynamic viscosity of synovial fluid has the value of η_0 = 0.50 Pas, the density of synovial fluid ρ = 1010 kg/m^3, the angular velocity of spherical bone head ω = 1.5 s^{-1}, the minimum value of gap height min(ε_{T1s})

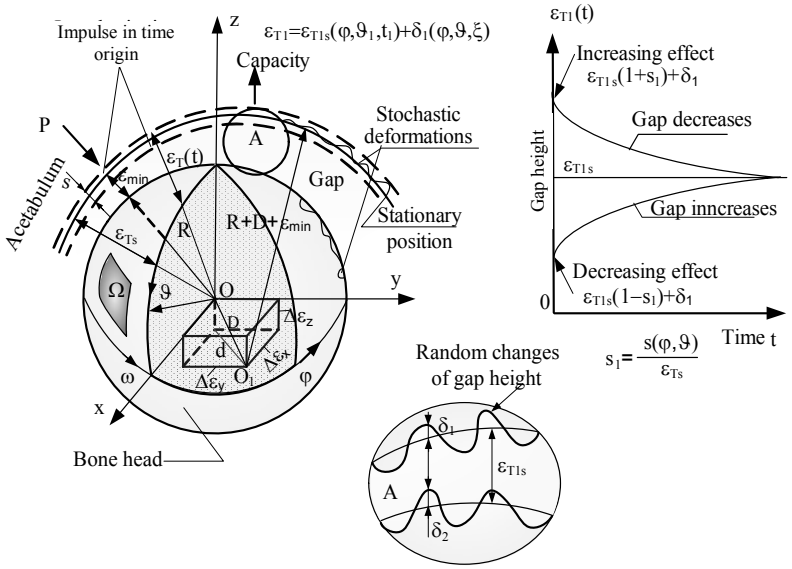

Fig. 6. Geometry of spherical bone head and hip joint gap with time after injury

The dimensionless function:

$$s_1 = \frac{s(\varphi,\vartheta_{1s})}{\varepsilon_{Ts}(\varphi,\vartheta_1)} \quad \text{for} \quad \vartheta_{1s} \equiv \frac{\vartheta_s}{R}, \quad \vartheta_1 \equiv \frac{\vartheta}{R} \qquad (43)$$

describes the gap-height changes during the impulsive motion caused by the force applied. The gap height increases if $s_1 > 0$, and decreases if $s_1 < 0$. The symbol ω_0 denotes an angular velocity in s^{-1} and describes the changes of time perturbations in unsteady flow of synovial fluid in the joint gap-height direction. If dimensionless time t_1 increases, then for $s_1 > 0$ the enlarged gap-height decreases, and in a sufficiently long time after impulse it attains the same time-independent value ε_{Ts}. If the dimensionless time t_1 increases, then for $s_1 < 0$ the reduced gap-height increases. In a sufficiently long time after impulse, the gap attains the same time-independent value ε_{Ts}.

Numerical calculations are performed in Matlab 7.2 and Mathcad 12 Professional Programs by means of the finite difference method for the radius of spherical bone head R = 0.0265 m, the angular velocity ω_0 = 0.15 s^{-1} of the impulsive perturbations of the gap changes within the time interval of 0.000001 s ≤ t ≤ 100 s, and attains the values within the range from 0.435 (4.35 μm) to 0.726 (7.26 μm). The average relative radial clearance has the value of $\psi \equiv \varepsilon_0/R$ = 3.774·10^{-4}. The characteristic dimensional pressure $p_0 = \omega\eta_0/\psi^2$ attains the value of 5.267 MPa. The characteristic dimensional gap-height value ε_0 equals 10 μm, the Strouhal number Str = 666666 and $Re\cdot\psi\cdot Str$ = 0.202. For the dimensionless times: $t_1 = 1$, $t_1 = 10^6$, $t_1 = 10^8$, i.e. for the dimensional times: t = 0.000001 s; t = 1.0 s; t = 100.0 s, respectively, and for $s_1 = \pm 0.25$ we obtain the distributions of dimensionless pressure given in figures 7 and 8. To obtain real values of time we must multiply the dimensionless values t_1 by the characteristic time value t_0 = 0.000001 s. For example, $t_1 = 10^6$ denotes 1 s after impulse. To obtain a dimensional value of pressure we must multiply the dimensionless pressure values (see figures 7 and 8) by the characteristic pressure value p_0. Figure 7 presents the dimensionless pressure values without random effects for $\sigma_{s1} = 0$. The dimensionless pressure values shown in figure 8 are obtained for stochastic gap-height

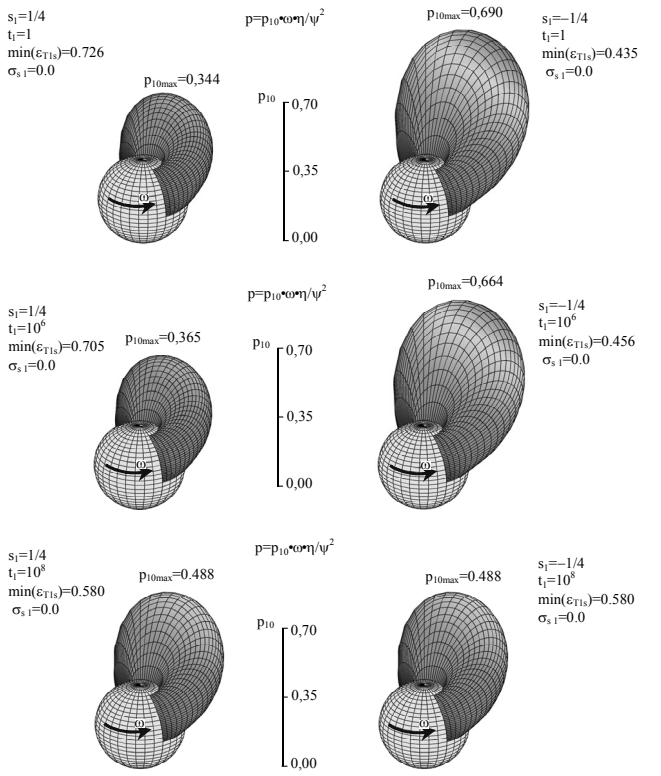

Fig. 7. Dimensionless hydrodynamic pressure distributions inside the gap of human spherical hip joint in the region Ω: $0 \le \varphi \le \pi$, $\pi R/8 \le \vartheta \le \pi R/2$ without stochastic changes ($\sigma_{s1} = 0$) in the dimensionless times: $t_1 = 1$ (i.e. $t = 0.000001$ s), $t_1 = 10^6$ (i.e. $t = 1$ s), $t_1 = 10^8$ (i.e. $t = 100$ s), after the impulse moment. For the increasing (decreasing) effects of gap-height changes see the left (right) column of the figures, respectively. The results are obtained for the following data: $R = 0.0265$ m; $\eta_0 = 0.50$ Pas; $\rho = 1010$ kg/m^3; $\varepsilon_0 = 10$ μm, $\Delta\varepsilon_x = 4$ μm; $\Delta\varepsilon_y = 0.5$ μm; $\Delta\varepsilon_z = 3$ μm; $\psi \equiv \varepsilon_0/R = 3.774 \cdot 10^{-4}$; $\omega = 1.5$ s^{-1}; $\omega_0 = 0.15$ s^{-1}; $Str = 666666$; $Re \cdot \psi \cdot Str = 0.202$

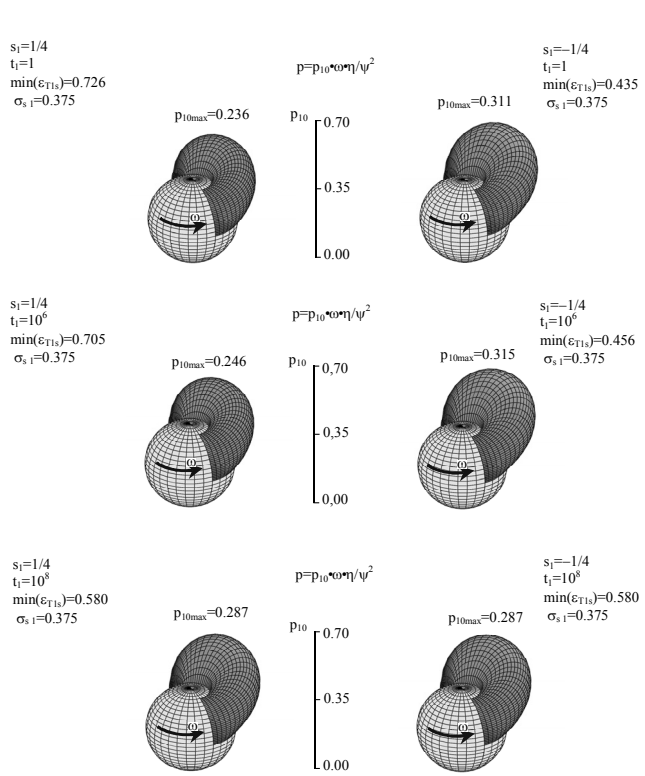

Fig. 8. Dimensionless hydrodynamic pressure distributions inside the gap of human spherical hip joint in the region Ω: $0 \le \varphi \le \pi$, $\pi R/8 \le \vartheta \le \pi R/2$ for stochastic changes with the standard deviation $\sigma_{s1} = 0.375$ (i.e. 0.37 μm) in the dimensionless times: $t_1 = 1$ (i.e. $t = 0.000001$ s), $t_1 = 10^6$ (i.e. $t = 1$ s), $t_1 = 10^8$ (i.e. $t = 100$ s), after the impulse moment. For the increasing (decreasing) effects of gap-height changes see the left (right) column of the figures, respectively. The results are obtained for the following data: $R = 0.0265$ m; $\eta_0 = 0.50$ Pas; $\rho = 1010$ kg/m^3; $\varepsilon_0 = 10$ μm; $\Delta\varepsilon_x = 4$ μm; $\Delta\varepsilon_y = 0.5$ μm; $\Delta\varepsilon_z = 3$ μm; $\psi \equiv \varepsilon/R \approx 3.774 \cdot 10^{-4}$; $\omega = 1.5$ s^{-1}; $\omega_0 = 0.15$ s^{-1}; $Str = 666666$; $Re \cdot \psi \cdot Str = 0.202$

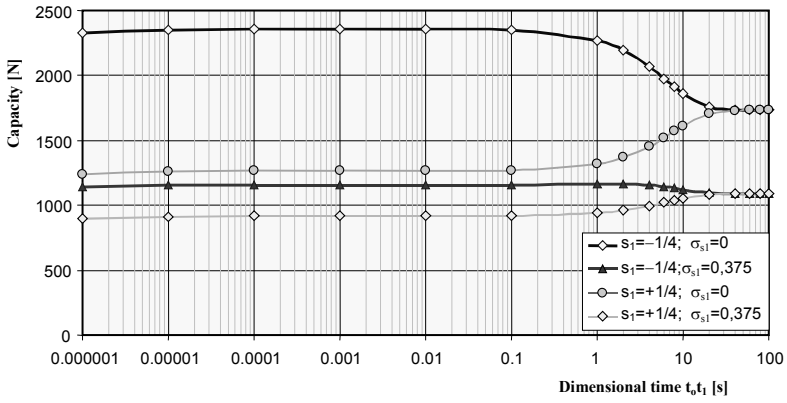

Fig. 9. Dimensional values of load carrying capacity versus dimensional time in the range from 10^{-6} second to 100 seconds after impulse inside the gap of human spherical hip joint in the region Ω: $0 \le \varphi \le \pi$, $\pi R/8 \le \vartheta \le \pi R/2$ for stochastic changes of roughness of cartilage surface with the standard deviation $\sigma_{s1} = 0.375$ (i.e. 0.37 μm) and without random effects for $\sigma_{s1} = 0$. The results are obtained for the following data: $R = 0.0265$ m; $\eta_0 = 0.50$ Pas; $\rho = 1010$ kg/m^3; $\varepsilon_0 = 10$ μm; $\Delta\varepsilon_1 = 4$ μm; $\Delta\varepsilon_2 = 0.5$ μm; $\Delta\varepsilon_3 = 3$ μm; $\psi \equiv \varepsilon_0/R = 3.774 \cdot 10^{-4}$; $\omega = 1.5$ s^{-1}; $\omega_0 = 0.15$ s^{-1}; $t_0 = 0.000001$ s; $Str = 666666$; $Re \cdot \psi \cdot Str = 0.202$

changes at $\sigma_{s1} = 0.375$. The distributions of dimensionless pressure presented for $s_1 > 0$ on the left-hand side of figures 7 and 8 are obtained for the marked effect of gap height caused by impulsive motion. In

this case, if the time after the impulse increases, then the gap height decreases and the pressure increases, and in a sufficiently long time after impulse it tends to the time-independent pressure.

The pressure distributions presented for $s_1 < 0$ on the right side in figures 7 and 8 are obtained for the reduced effect of gap height caused by impulsive motion. In this case, if the time after the impulse increases, then the gap height increases and the pressure decreases and in a sufficiently long time after impulse it tends to the time-independent pressure. Figure 9 presents the dimensional value of load carrying capacity for human hip joint versus the dimensional time ranging from the beginning of the impulse to 100 s after the impulse.

8. Conclusions

Examining the effect of the shape of cylindrical and conical biobearings in human joints on the pressure and load carrying capacity distributions leads to the following conclusions:

1. If the angle γ between conical surface and the cross section plane increases in conical biobearing, then the capacity increases in cross-wise direction and decreases in longitudinal direction.

2. At the same angular velocities and synovial fluid dynamic viscosities and for similar geometries, i.e. for the same eccentricities, the maxima of hydrodynamic pressure in biobearing of the cylindrical shapes of boneheads exceed the maxima of hydrodynamic pressures in biobearing of the conical shapes of boneheads.

3. Contrary to the biobearings with cylindrical boneheads, the biobearings with conical boneheads have carrying capacities in two directions.

Studying the effect of the unsteady lubrication of spherical hip joint during the injury and impulsive flow on the load carrying capacity and pressure distribution with optimal standard deviation arrives at the following conclusions:

1. If the gap height ($s_1 > 0$) of a normal joint grows as a result of trauma, then just after an impulse the gap height decreases and the pressure increases. In a sufficiently long time after impulse, the gap height and the pressure attain the time-independent values. If the gap height decreases ($s_1 < 0$) as a result of trauma, then just after an impulse the gap height increases and the pressure decreases. In a sufficiently long time after an impulse, the gap height and the pressure reach the time-independent values.

2. If the time after the impulse is long enough, i.e. for $t_1 \to \infty$, and if we take into account the optimal standard deviations of the gap height, then the pressure distributions for the increasing ($s_1 > 0$) and decreasing ($s_1 < 0$) effects of the gap-height changes caused by the impulse are almost the same. This limit pressure distribution can also be obtained from the stochastic Reynolds equation (13) for the arbitrary standard deviation σ_{s1}.

3. From the numerical calculations we conclude that the pressure and the load carrying capacity of the joint, obtained for the optimal standard deviation $\sigma_{s1} = 0.375$ by virtue of the measurements of the roughness of normal cartilage surfaces of the human hip joint, decrease by about 30% in comparison with the pressure and the load carrying capacity obtained for smooth cartilage surface without asperities and random effects.

4. The numerical calculations show that the biggest changes of pressure distribution and capacity in human joint occur within the time interval from 0.1 s to 30 s after an impulse.

Acknowledgement

This research project has been supported by the Marie Curie Transfer of Knowledge Fellowship of the European Community's Sixth Framework Program under contract number MTKD-CT-2004-517226.

References

[1] ASADA T. et al., *Hydrodynamic bearings and applied technologies*, Matsushita Tech., 2000, 46 (1), 54–76.

[2] CHUN-YUH HUANG, SOLTZ MICHAEL A., KOPACZ M., MOW VAN C., ATESHIAN G.A., *Experimental verification of the roles of intrinsic matrix viscoelasticity and tension–compression nonlinearity in the biphasic response of cartilage*, ASME, Journal of Biomechanical Engineering, 2003, Vol. 125, No. 1, 84–93.

[3] FRECHETTE L.G., JACOBSON S.A., BREUEN K.S. et al., Journal MEMS, 2005, 14, 141–152.

[4] FUNG Y.C., *Biomechanics, Motion, Flow, Stress and Growth*, Springer Verlag, New York, Hong Kong, 1993.

[5] FUNG Y.C., *The Meaning of Constitutive Equations in Biomechanics, Mechanical Properties of Living Tissues*, Springer Verlag, Berlin, 1993.

[6] FYHRIE D.P., BARONE J.R., *Polymer dynamics as a mechanistic model for the flow-independent viscoelasticity of cartilage*, Trans. of the ASME, October 2003, Vol. 125, 578–584.

[7] HYC A., OSIECKA-IWAN A., JÓŹWIAK J., MOSKALEWSKI S., *The morphology and selected biological properties of articular cartilage*, Ortopedia, Traumatologia, Rehabilitacja, 2001, Vol. 3, No. 2, 151–162.

[8] STOCKWELL R.A., *Biology of cartilage cells*, Cambridge University Press, Cambridge, 1979.

[9] TRICKEY T.R., LEE M., GUILAK T., *Viscoelastic properties of chondrocytes from normal and osteoarthritic human cartilage*, Journal Orthop. Res., 2000, 18, 891–898.

[10] TRUCKENBRODT E., *Strömungsmechanik*, Springer Verlag, New York, Berlin, 1986.
[11] TRUESDELL C., *A First Course in Rational Continuum Mechanics*, Baltimore, Maryland, Hopkins University, 1972.
[12] WIERZCHOLSKI K., *Random changes of temperature in slide bearing gap*, International Congress, Thermal Stress IUTAM Proceedings, Vienna, 2005, 449–452.
[13] WIERZCHOLSKI K., *Boundary conditions on the bio-cell surfaces for nano-lubrication of micro-bearings*, J. of Kones Powertrain and Transport, 2007, Vol. 14, No. 3, 603–609.
[14] WIERZCHOLSKI K., *Bio and slide bearings; their lubrication by non-Newtonian fluids and application in non-conventional systems*, Vol. I and Vol. III, Second Edition: (I) *Principles of Human Joint Lubrication*, (III) *Tribology Processes for Cells, Human Joints and Microbearings*, Monograph, Gdańsk University of Tech., 2006.
[15] WIERZCHOLSKI K., *Hip joint lubrication after injury for stochastic description with optimum standard deviation*, Acta of Bioengineering and Biomechanics, 2005, Vol. 7, No. 2, 13–40.
[16] WIERZCHOLSKI K., *Lubrication of deformed hip joint*, International Conference System Modelling and Control, Zakopane, 2007, 1–8.
[17] WIERZCHOLSKI K., MISZCZAK A., *Flow on the biocell surfaces as an element of the microbearing tribology*, Journal of Kones Powertrain and Transport, 2007, Vol. 14, No. 2, 553–560.
[18] www.oce.pg.gda.pl/biobearing/?path=8, 2006.
[19] WIERZCHOLSKI K., MISZCZAK A., *Load carrying capacity of microbearing with parabolic bone head*, Journal of Solid State Phenomena, Vols. Mechatronic Systems and Materials III, 2008/2009, Vols. 147–149, 542–547.